



A second-order immersed boundary method for the numerical simulation of two-dimensional incompressible viscous flows past obstacles.

François Bouchon, Thierry Dubois, Nicolas James

► To cite this version:

François Bouchon, Thierry Dubois, Nicolas James. A second-order immersed boundary method for the numerical simulation of two-dimensional incompressible viscous flows past obstacles.. 2010. hal-00570090

HAL Id: hal-00570090

<https://hal.science/hal-00570090>

Preprint submitted on 26 Feb 2011

HAL is a multi-disciplinary open access archive for the deposit and dissemination of scientific research documents, whether they are published or not. The documents may come from teaching and research institutions in France or abroad, or from public or private research centers.

L'archive ouverte pluridisciplinaire **HAL**, est destinée au dépôt et à la diffusion de documents scientifiques de niveau recherche, publiés ou non, émanant des établissements d'enseignement et de recherche français ou étrangers, des laboratoires publics ou privés.

A second-order immersed boundary method for the numerical simulation of two-dimensional incompressible viscous flows past obstacles

François Bouchon, Thierry Dubois and Nicolas James

Abstract We present a new cut-cell method, based on the MAC scheme on cartesian grids, for the numerical simulation of two-dimensional incompressible flows past obstacles. The discretization of the nonlinear terms, written in conservative form, is formulated in the context of finite volume methods. While first order approximations are used in cut-cells the scheme is globally second-order accurate. The linear systems are solved by a direct method based on the capacitance matrix method. Accuracy and efficiency of the method are supported by numerical simulations of 2D flows past a cylinder at Reynolds numbers up to 9 500.

1 Introduction

Avoiding the use of curvilinear or unstructured body-conformal grids, immersed boundary (IB) methods provide efficient solvers, in terms of computational costs, on Cartesian grids for flows in complex geometries. IB methods can be classified in two groups. Classical IB methods add in the momentum equation a forcing term accounting for the presence of a solid obstacle in the computational domain. Cut-cell methods discretize the momentum and continuity equations in mesh cells cut by the solid. The scheme proposed in this paper lies in this class of IB methods and differs from other cut-cell methods in the treatment of the diffusive and convective terms in cut-cells. The scheme is globally second-order accurate for the velocity and pressure variables.

This paper is organized as it follows. The first section is devoted to the description of the problem. Then the IB/cut-cell method is detailed and finally some numerical simulations are given.

Laboratoire de Mathématiques, Université Blaise Pascal and CNRS (UMR 6620), Campus Universitaire des Cézeaux, 63177 AUBIERE, France, e-mail: name.surname@math.univ-bpclermont.fr

2 The settings of the problem

Let Ω be a rectangular domain. We consider an irregular fluid domain Ω^F which is embedded in the computational domain Ω and its complement Ω^S , the solid domain. The interface between solid and fluid is denoted Γ . The decoupling between velocity and pressure variables is achieved by applying a second-order (BDF) projection scheme to the incompressible Navier-Stokes equations. First, the *prediction step* consists in computing the velocity field \mathbf{u}^{k+1} which is solution of the following equation :

$$\frac{3\tilde{\mathbf{u}}^{k+1} - 4\mathbf{u}^k + \mathbf{u}^{k-1}}{2\delta t} - \triangle \tilde{\mathbf{u}}^{k+1}/Re = -\nabla p^k + \mathbf{f}^{k+1} - 2 \operatorname{div}(\mathbf{u}^k \otimes \mathbf{u}^k) \quad (1)$$

$$+ \operatorname{div}(\mathbf{u}^{k-1} \otimes \mathbf{u}^{k-1}) \quad (2)$$

with appropriate boundary conditions on $\partial\Omega^F$. Then we solve the *projection step* :

$$\mathbf{u}^{k+1} = \tilde{\mathbf{u}}^{k+1} - \frac{2\delta t}{3} \nabla(p^{k+1} - p^k), \quad (3)$$

$$\operatorname{div} \mathbf{u}^{k+1} = 0, \quad (4)$$

$$(\mathbf{u}^{k+1} - \tilde{\mathbf{u}}^{k+1})|_{\partial\Omega} \cdot \mathbf{n} = 0. \quad (5)$$

3 The IB/cut-cell method

3.1 Staggered arrangement of the unknowns

As in Cheny and Botella [1], a signed distance to the obstacle d is used to represent solid boundaries in the computational domain. The pressure is placed at the center of every cartesian cell either filled by the fluid or cut by the solid boundaries (see Figure 1). The velocity components are placed at the middle of the part of the edges located in the fluid. Unlike for cells located in the fluid part of the computational domain, velocity and pressure are not aligned in cut-cells. Cell-face ratios $r_{i,j}^u, r_{i,j}^v$ are calculated from the distance of the mesh point to the obstacle, denoted $d_{i,j}$. The interface Γ_h , linear in each cell, approaches the regular solid boundary Γ (see Figure 1).

3.2 Discretization of the prediction step

In fluid cells, the classical five-point stencil approximation of the viscous terms is used. In cells sharing a face with a cut-cell, we propose a first-

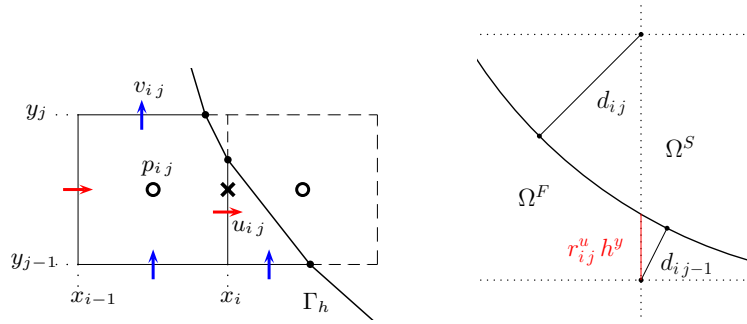


Fig. 1 Staggered arrangement of the unknowns in cells cut by an obstacle

order Finite Difference approximation. More precisely, we consider $\mathcal{V} = \{O, N, S, E, W, P\}$ with O the position of $u_{i,j}$, N, S, E, W are the location of unknowns close to O or on the boundary, and P is arbitrarily chosen (see Figure 2). Then, we search coefficients α_M such that $\sum_{M \in \mathcal{V}} \alpha_M u(M)$ is a first

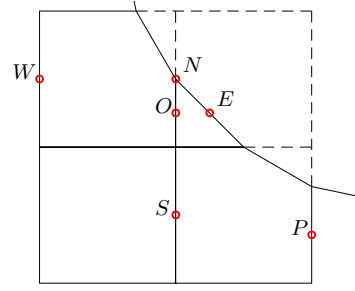


Fig. 2 Six points are used for the discretization of the diffusive term in mesh cells cut by the solid boundary

order approximation of $\Delta u(O)$. This leads to a linear system of six equations with six unknowns.

In fluid cells, a second-order centered approximation for the nonlinear terms is used. In cells sharing a face with a cut-cell, we propose a first-order Finite Volume approximation of nonlinear terms. The integral of the first component of the nonlinear term over a cut-cell $\tilde{K}_{i,j}^u = K_{i,j}^u \cap \Omega_h^F$ is expressed in terms of fluxes through cell edges, namely :

$$\int_{\tilde{K}_{i+\frac{1}{2},j}} (\partial_x(u^2) + \partial_y(uv)) d\mathbf{x} = \int_{\partial \tilde{K}_{i+\frac{1}{2},j}} (u^2 n_x + (uv) n_y) dS \quad (6)$$

$$= F_{i+1,j}^E - F_{i,j}^E + F_{i,j}^N - F_{i,j-1}^N + F_{i,j}^B. \quad (7)$$

Second-order interpolations of velocity components are used to approximate the fluxes at the center of cut-edges (see Figure 3). This leads to a pointwise first-order approximation of the convective terms.

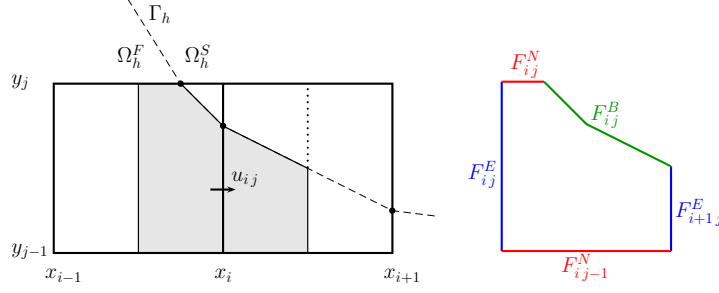


Fig. 3 Discretization of the convective term using fluxes reconstruction

3.3 Discretization of the projection step

The continuity equation is decomposed as the net mass flux through each face of the computational cells. Due to the locations of velocity components, a second-order approximation follows immediately. The discretization of (4) on a cut-cell is $(D_{obs} \mathbf{u})_{i,j} = (D_{obs}^0 \mathbf{u})_{i,j} + D_{i,j}^{supp} = 0$, where the linear part of the discrete divergence is

$$(D_{obs}^0 \mathbf{u})_{i,j} = h_y(r_{i,j}^u u_{i,j} - r_{i-1,j}^u u_{i-1,j}) + h_x(r_{i,j}^v v_{i,j} - r_{i,j-1}^v v_{i,j-1}) \quad (8)$$

and the contribution to the divergence due to the boundaries is $D_{i,j}^{supp} = \ell_{i,j} \mathbf{g}(M) \cdot \mathbf{n}_{i,j}$. Note that $\ell_{i,j}$, M and $\mathbf{n}_{i,j}$ are respectively the length, the middle point and the external normal of the edge of the cut-cell shared with the boundary (see Figure 1). In the case of a fluid cell, this expression reduces to the standard MAC discretization.

The velocity correction step requires the computation of the pressure gradients at the location of the velocity. For faces cut by solid boundaries, a second-order interpolation \mathcal{P}_ϕ is used. As in the classical MAC scheme, a discrete Poisson-type equation for the pressure increment $\delta p^{k+1} = p^{k+1} - p^k$ is obtained by applying the discrete divergence operator to the velocity correction equations :

$$D_{obs}^0(\mathcal{P}_\phi(G\delta p^{k+1})) = \frac{3}{2} \frac{h^2}{\delta t} D_{obs}(\tilde{\mathbf{u}}^{k+1}), \quad (9)$$

with the classical discrete gradient

$$(G\delta p^{k+1})_{i,j} = \left((\delta p_{i+1,j}^{k+1} - \delta p_{i,j}^{k+1})/h_x, (\delta p_{i,j+1}^{k+1} - \delta p_{i,j}^{k+1})/h_y \right). \quad (10)$$

It follows that the velocity correction

$$\mathbf{u}^{k+1} = \tilde{\mathbf{u}}^{k+1} - \frac{2}{3} \frac{\delta t}{h^2} \mathcal{P}_\phi(G\delta p^{k+1}) \quad (11)$$

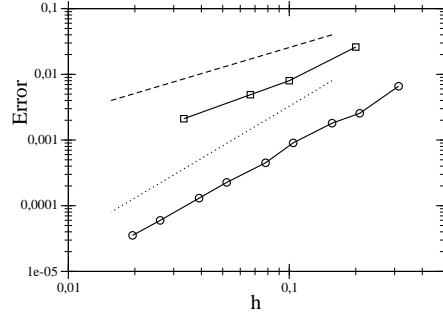
ensures that the incompressibility condition $D_{obs}(\mathbf{u}^{k+1}) = 0$ is satisfied in the whole domain up to computer accuracy.

3.4 Computational efficiency

The non-symmetric linear systems are efficiently solved by a direct method, based on the capacitance matrix method [2]. First, we solve a preprocessing step, requiring $\mathcal{O}(n^3)$ operations. Assuming that the obstacle does not move, this step is solved once per simulation. Then, at every time step, this technique allows to reduce the overall cost of the resolution to $\mathcal{O}(n^2 \log(n))$ operations, which is the number of operations needed to solve the linear systems corresponding to five-point stencil operators on the whole cartesian mesh without obstacle.

The method is tested on the Taylor-Couette flow between two concentric cylinders : second-order spatial convergence for velocity and pressure is found. In Figure 4, we have reported the L^∞ error for the velocity, when the error is measured on the whole fluid computational domain. Unlike in [1], the second-order accuracy is also satisfied in cut-cells.

Fig. 4 Error for the velocity versus grid size h . Present study (circles), Cheny and Botella results [1] (squares), first-order slope (dash) and second-order slope (dotted).



Numerical simulations of 2D flows past a cylinder have been performed at Reynolds numbers up to 9 500. As it is shown on Figure 5, an excellent agreement is found with the experimental results presented in Bouard and Coutenceau [3]. Streamlines of the flow past a cylinder at $Re = 9\,500$ at time $t = 0.75, 1.0$ and 1.25 are represented on Figure 5. We have also studied the flow past a NACA aerofoil at $Re = 1\,000$. Like in [4], a Karman vortex street develops behind the obstacle (see Figure 6) : the flow is well resolved even near the sharp ending edge. For these numerical simulations, the mesh size near the obstacle is $1.6 \cdot 10^{-3}$. The value of the time step, satisfying a CFL stability condition, is 10^{-4} .

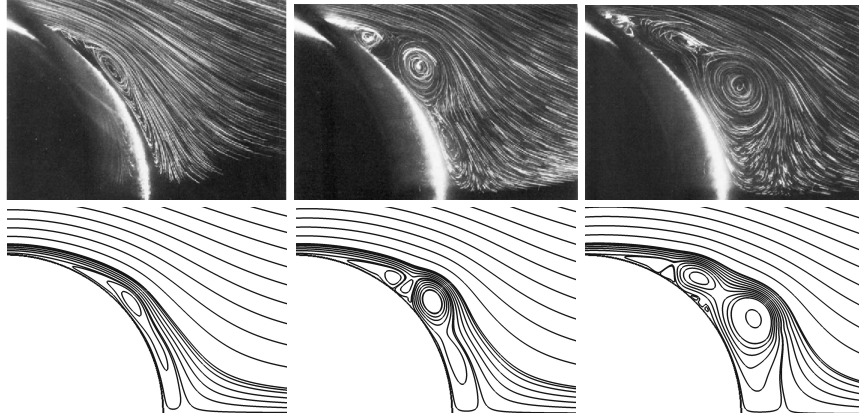


Fig. 5 Evolution of the boundary layer : comparison with experimental results at $Re = 9\,500$.

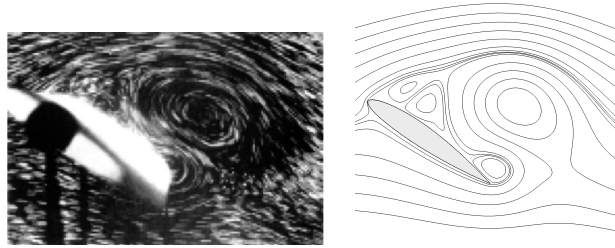


Fig. 6 Flow behind a NACA aerofoil at $Re = 1\,000$: comparison with experimental results.

References

1. Yoann Cheny and Olivier Botella : The LS-STAG method: A new immersed boundary/level-set method for the computation of incompressible viscous flows in complex moving geometries with good conservation properties. *J. of Comput. Phys.* **229**–4, 1043–1076 (2010)
2. B.L. Buzbee, F.W. Dorr, J.A. George and G.H. Golub : The direct solution of the discrete Poisson equation on irregular regions. *J. Num. Anal.* **8**, 722–736 (1971)
3. R. Bouard and M. Coutanceau : The early stages of development of the wake behind an impulsively started cylinder for $40 < Re < 10^4$. *J. Fluid. Mech.* **101**, 583–607 (1980)
4. O. Daube, Ta Phuoc Loc, P. Monnet and M. Coutanceau : Ecoulement instationnaire decolle dun fluide incompressible autour dun profil : une comparaison theorie - experience, AGARD CP **386**, Paper 3, (1985)